Intrinsic valley polarization of magnetic VSe_2 monolayers

2017 J. Phys.: Condens. Matter 29 255501

(http://iopscience.iop.org/0953-8984/29/25/255501)

IOP Publishing Journal of Physics: Condensed Matter
J. Phys.: Condens. Matter **29** (2017) 255501 (7pp) https://doi.org/10.1088/1361-648X/aa6e6e

Intrinsic valley polarization of magnetic VSe_2 monolayers

Jian Liu[1], Wen-Jie Hou[2], Cai Cheng[1], Hui-Xia Fu[1], Jia-Tao Sun[1] and Sheng Meng[1,3]

[1] Beijing National Laboratory for Condensed Matter Physics and Institute of Physics, Chinese Academy of Sciences, Beijing 100190, People's Republic of China
[2] Department of Physics, Renmin University of China, Beijing 100872, People's Republic of China
[3] Collaborative Innovation Center of Quantum Matter, Beijing 100190, People's Republic of China

E-mail: jtsun@iphy.ac.cn and smeng@iphy.ac.cn

Received 14 March 2017, revised 10 April 2017
Accepted for publication 21 April 2017
Published 18 May 2017

Abstract

Intrinsic valley polarization can be obtained in VSe_2 monolayers with broken inversion symmetry and time reversal symmetry. First-principles investigations reveal that the magnitude of the valley splitting in magnetic VSe_2 induced by spin–orbit coupling reaches as high as 78.2 meV and can be linearly tuned by biaxial strain. Besides conventional polarized light, hole doping or illumination with light of proper frequency can offer effective routes to realize valley polarization. Moreover, spin–orbit coupling in monolayer VSe_2 breaks not only the valley degeneracy but also the three-fold rotational symmetry in band structure. The intrinsic and tunable valley splitting and the breaking of optical isotropy bring additional benefits to valleytronic and optoelectronic applications.

Keywords: intrinsic valley splitting, valley polarization, spin–orbit coupling, optical anisotropy

S Supplementary material for this article is available online

(Some figures may appear in colour only in the online journal)

1. Introduction

Energy valley is the extreme point of energy dispersion in solid crystals. The energy extremum valley in band structures is considered as a new degree of freedom of electrons with the capability to manipulate the movement of electrons in a controlled way, fostering valleytronics in analogy with spintronics. For example, graphene, a hexagonal carbon monolayer, has two valleys K_+ and K_-. The two energy-degenerate but non-equivalent valleys in non-magnetic materials (such as graphene) can be used as a discrete degree of freedom because of the large valley separation in momentum space. According to the semiclassical theory, which includes the Berry phase correction to the group velocity of electronic structure band dispersion, the movement of the electron wave packet is

$$\dot{r} = \frac{1}{\hbar}\frac{\partial E_n(k)}{\partial k} - \frac{e}{\hbar}E \times \Omega(k),$$

where E is the applied electric field and $\Omega(k)$ is the momentum dependent Berry curvature summing over all occupied states [1–3]. The valley Hall effect can be accessed by transport experiments where charge carriers at two different valleys flow to the opposite transverse direction driven by the non-vanishing Berry curvature $\Omega(k)$ in the nonequilibrium electron occupation of both valleys [4–6]. The massive Dirac fermion inherited from graphene and transition metal dichalcogenide MX_2 (M = Mo, W; X = S, Se, Te) monolayers with broken inversion symmetry (IS) emerges as prototypical candidate for valley Hall effect.

The valley polarization of a material is usually dependent strongly on external magnetic fields or proximity-induced interactions of magnetic substrate, making it very difficult to achieve intrinsic valley polarization without external perturbation. A nonequilibrium valley carrier can be obtained via circular dichroism under the constraint of valley dependent optical selection rules, namely conservation of angular

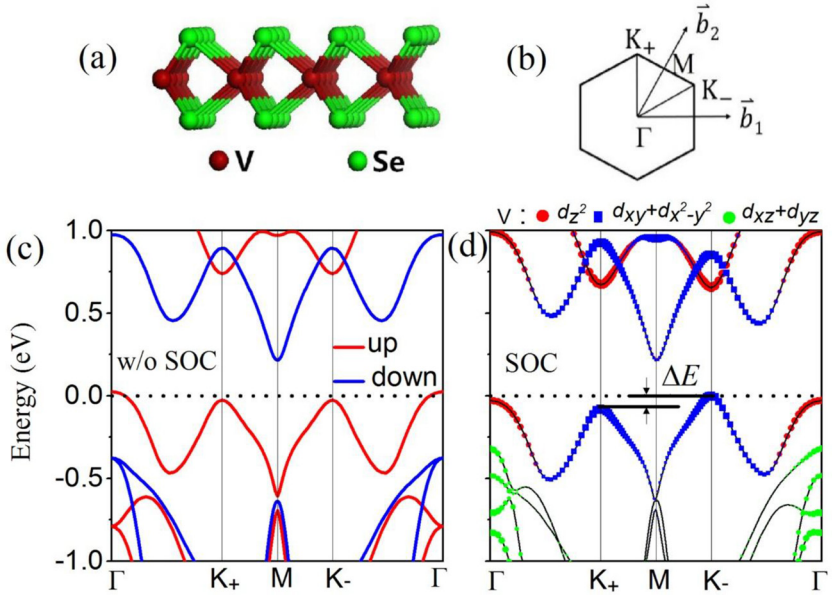

Figure 1. Atomic and electronic structures of 2H–VSe_2. (a) Geometric structure of VSe_2 in side view. (b) Schematic diagram of the 2D first Brillouin zone with special k points along high symmetry line. (c) Spin-polarized band structures calculated by PBE methods. Spin-up (spin-down) bands are denoted by red (blue) lines respectively. (d) Orbital projected band structures with spin–orbit coupling calculated with PBE methods. Red circle, blue square and green circles represent d_{z^2}, $d_{xy}+d_{x^2-y^2}$, $d_{xz}+d_{yz}$ orbital composition respectively. The sizes of dots denote the weight of contribution.

momentum [7–9]. A few recent experiments show only small valley splitting can be generated in the presence of an external magnetic field in monolayer $MoSe_2$, $MoTe_2$, WSe_2 materials and other nonmagnetic materials [10–22]. Although the valley splitting induced by the proximity-induced Zeeman effect can reach 300 meV in $MoTe_2$/EuO heterostructure [23, 24], a magnetic substrate possessing a large magnetism is essential and no experiment at present shows the possibility of material growth. The intrinsic valley polarization without external perturbation (magnetic field) is still missing.

Vanadium disulfides/diselenides are members of transition metal dichalcogenide compounds, with interlayer interaction coming from weak van der Waals forces. Similar to MoS_2, vanadium disulfide compounds also have two phases, namely 2H phase belonging to D_{3h} point group with mirror symmetry and 1T phase with IS, respectively. In contrast to MoS_2, however, VS_2 has an intrinsic magnetic moment [25, 26] and shows an electronic transition from metallicity to semiconducting because of the quantum size effect. Although phase transition between 2H and 1T can be realized via temperature control or applying strain, 2H structure is usually more stable up to high temperatures [27, 28]. Recently, ultrathin VS_2 nanosheet stacked with less than five layers and an approximately 0.4 nm thick VSe_2 monolayer nanosheet have been successfully synthesized [29, 30], providing a real material candidate to explore intrinsic valley properties without external magnetic field [31].

In this work, we study the electronic properties of a 2H–VSe_2 monolayer with broken IS and time reversal symmetry (TRS) by using first-principles calculations. We found that in such a magnetic two-dimensional (2D) material, the bands at the two non-equivalent valleys are degenerate without spin–orbit coupling (SOC) effect. However, after taking the SOC into consideration, the bands at the two valleys have a large energy splitting, indicating the degeneracy of valley degree of freedom is spontaneously broken. The intrinsic valley splitting reaches as high as 78.2 meV, which is large enough to be easily measurable in experiment. The intrinsic breaking of valley degeneracy will induce Berry curvature at two different valleys with unequal absolute values. Besides conventional approaches using circularly polarized light, valley polarization can also be obtained by either carrier doping or light illumination with proper photon energy, thanks to the existence of intrinsic valley splitting. Interestingly, the SOC effect breaks not only the valley degeneracy, but also the three-fold rotational symmetry from the analysis of band structure and anisotropic optical absorption.

2. Methods

All calculations were performed in the framework of density functional theory using the Vienna *Ab Initio* Simulation Package (VASP) [32]. Interactions between valence electrons and ionic cores were described with the projector augmented wave (PAW) method [33, 34]. We adopted the generalized gradient approximation of Perdew–Burke–Ernzerhof (PBE) and hybrid HSE06 functional for the exchange-correlation energy [35, 36]. A plane wave basis set with a cutoff energy of 400 eV was used to expand the wave functions. The 2D Brillouin zone (BZ) integration was sampled by a 24 × 24 × 1 k-grid mesh for calculations of electronic properties [37]. A vacuum layer with a thickness larger than 15 Å was set in the calculation for monolayer VSe_2 to ensure decoupling between periodic VSe_2 layers. For structural relaxation, all the atoms were allowed to relax until the atomic force on each atom was smaller than 0.001 eV $Å^{-1}$. Both the lattice constant and the

atomic positions were fully optimized. The HSE06 calculations were also carried out to verify the results. The standard exact-exchange mixing parameter $\alpha = 0.1$ was used for the HSE06 functional to keep the same trend of band obtained from PBE and HSE06. The SOC effect [38] was explicitly included in the calculations. The Berry curvature and Fermi surface were calculated at a dense enough mesh by *ab initio* tight binding method, using maximally localized Wannier functions (MLWF) implemented in Wannier90 code [39]. Five *d* orbitals for each V atom and three *p* orbitals for each Se atom have been used to construct a real space Hamiltonian in the Wannier basis.

3. Results

The 2H monolayer VSe_2 has the D_{3h} point-group symmetry as shown in figure 1(a). In such a monolayer, an intermediate layer of hexagonally arranged V atoms is sandwiched between two layers of Se atoms. Each V atom is surrounded by six Se atoms, and each Se atom has three nearest neighbor V atoms. The optimized lattice constant is 3.33 Å, and the angle of Se–V–Se is 79.1 degrees. The magnetic moment of each V atom is calculated to be 1 μ_B, consistent with previous results [25]. The ferromagnetic (FM) state is energetically more favorable than the antiferromagnetic (AFM) state by the energy difference $\Delta E_{FM-AFM} = -76.1$ meV. Then the Curie temperature T_C is estimated to be about 588 K via the mean-field approximation and Heisenberg model using the relation $\frac{3}{2}K_BT_C = -\Delta E_{FM-AFM}$ [40]. In figure 1(b) the first BZ with the corresponding high symmetry points is plotted, where two non-equivalent valleys are designated as K_+ and K_-, respectively. The band structure without and with the SOC effect are shown in figures 1(c) and (d). The calculated band structure of 2H monolayer VSe_2 shows that the bands right below the Fermi level is spin polarized with a majority (spin-up) component. The indirect energy band gap between occupied spin-up bands and unoccupied spin-down bands is 0.19 eV in PBE and 0.69 eV in HSE06 calculations (SI, figure S1 (stacks.iop.org/JPhysCM/29/255501/mmedia)).

When the SOC is turned on, we found that the degeneracy of the energy bands near the Fermi level at the two non-equivalent valleys is broken. The valley splitting, defined as $\Delta E = |E(K_+) - E(K_-)|$, where $E(K_+)$ ($E(K_-)$) is the energy of the valence band at K_+ (K_-) valley, is 78.2 meV by using PBE exchange-correlation functional and 112.1 meV if the hybrid HSE06 functional is used, equivalent to the case that a valley degenerate material is exposed to a 675 Tesla external magnetic field [24].

In order to understand why intrinsic valley energy splitting shows up in 2H monolayer VSe_2, we plot orbital-projected band structures around Fermi energy level in the energy window from −2 to 2 eV as shown in figure 1(d). The top (bottom) of valence (conduction) band is mainly contributed by d_{xy} and $d_{x^2-y^2}$ (d_{z^2}) orbitals of V atom at the *K* valleys. A similar composition is observed in other transition metal dichalgenides such as MoS_2. The wavefunction of V *d* orbitals can be rewritten in the form of spherical harmonics and the on-site contribution of SOC Hamiltonian operator is $H_{soc} = \xi\hat{L}\cdot\hat{S}$ [41]. Since the electron wavefunction can be reduced to the direct product of spin and orbital momentum and the off-diagonal orbital term $\langle d_{z^2}|H_{soc}|d_i\rangle$ ($i = xy,\ x^2-y^2$) is zero, usually only the spin channel coupled with the same magnetic quantum number can contribute to the SOC effect around K_+ and K_- valley. However, in VSe_2 the valence band around K_+ valley contains 0.24% contribution from V d_{xz}, d_{yz} orbitals, which is not found at all around the K_- valley. The orbital term $\langle d_{z^2}|H_{soc}|d_i\rangle$ $(i = xz, yz)$ and $\langle d_i|H_{soc}|d_j\rangle$ $(i = xz, yz; j = xy, x^2-y^2)$ is nonzero, therefore the spin term from different orbitals will also exist at the K_+ valley. The slight difference of orbital composition at two valleys plays a crucial role in the intrinsic breaking of valley degeneracy.

The tunability of valley splitting is of paramount importance for practical applications. Previous studies indicated that the valley splitting is tunable via the external magnetic field [12, 24]. Local strain can intrinsically enhance weak ferromagnetic ordering [25, 42], which may invoke a tunable valley splitting. To this aim, biaxial strain is adopted to realize a tunable valley splitting. The biaxial strain is defined as $\varepsilon = {}^{\Delta a}/_{a_0}$, where a_0 and $a = a_0 + \Delta a$ are the unstrained and strained lattice constants, respectively. The calculated valley splitting under strain at K_+ and K_- valley is shown in figure S2. It is found that the valley splitting, changing from 80 to 75 meV, is linearly dependent on the applied strain in the range of −2%–2%, indicating the significance of deformation potential [43].

The distinguishability of nonequivalent valleys is also associated with the valley contrasting Berry curvature besides the intrinsic valley splitting. Compared to the plane wave method, Wannier functions are computationally feasible to obtain the Berry curvature and Fermi surface, which should be calculated at a very dense mesh. Figure 2(a) shows the excellent agreement of the band structures obtained by DFT + SOC and Wannier functions, respectively. The Berry curvature of the *n*th band at *k* points along *z* direction perpendicular to the 2H–VSe_2 monolayer can be written as,

$$\Omega_n^z(k) = -\sum_{n'\neq n} \frac{2\mathrm{Im}\langle\psi_{nk}|v_x|\psi_{n'k}\rangle\langle\psi_{n'k}|v_y|\psi_{nk}\rangle}{(\varepsilon_{n'}-\varepsilon_n)^2}. \quad (1)$$

The Berry curvature of all occupied band defined as $\Omega^z(k) = \sum_n f_n\Omega_n^z(k)$ can be obtained by summing over occupied valence bands in Wannier basis. Here $v_x(v_y)$ is the velocity operator along the *x* and *y* direction and $f_n = 1$ for occupied bands [3].

We calculated the Berry curvature for the first BZ at a 500 × 500 *k*-point mesh as shown in figures 2(c) and (d). The calculated Berry curvature Ω^z is sharply peaked and shows opposite sign at K_+ and K_- valleys due to the lack of IS, which is similar to the results of 2H monolayer MoS_2, graphene and non-magnetic materials [4, 9, 44]. The key difference distinguishing 2H–VSe_2 from the above non-magnetic materials is the asymmetric distribution of Berry curvature. It is observed that the Berry curvature at K_+ valley has a smaller size but a

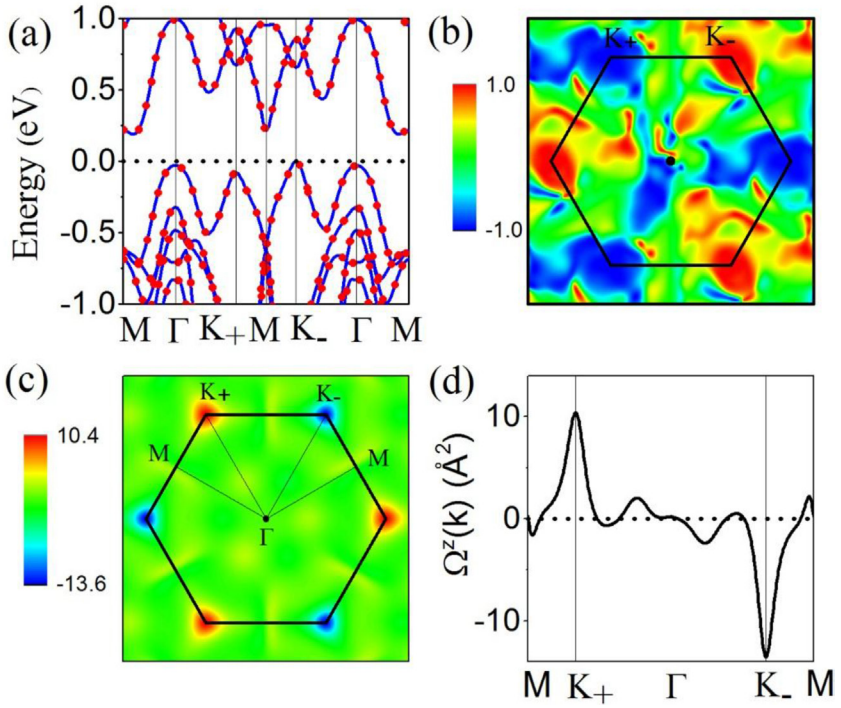

Figure 2. (a) The energy bands obtained from the DFT + SOC (blue) calculations overlaid by the Wannier interpolation (red dots). (b) The k-resolved degree of optical polarization $\eta(k)$. (c) Berry curvature for the occupied bands including the first Brillouin zone of 2H–VSe_2. (d) The Berry curvature along high symmetry points.

greater area of distribution compared to that at K_- valley, thus generating a zero Chern number.

To utilize valley degree of freedom for next-generation electronics, the key challenge lies in obtaining a non-equilibrium charge carrier imbalance at different valleys, namely, valley polarization [7]. Valley polarization can be achieved in 2D honeycomb materials via valley-contrasting circular dichroism [10–22]. The k-resolved degree of optical polarization $\eta(k)$ is given as [7, 9],

$$\eta(k) = \frac{\left|P_+^{cv}(k)\right|^2 - \left|P_-^{cv}(k)\right|^2}{\left|P_+^{cv}(k)\right|^2 + \left|P_-^{cv}(k)\right|^2} \tag{2}$$

where $P_\pm^{cv}(k) = \left\langle \psi_{ck} \middle| \hat{p}_x \pm i\hat{p}_y \middle| \psi_{vk} \right\rangle$ represents direct interband transition matrix for left or right polarized light, $\hat{p}_x$ ($\hat{p}_y$) is the momentum operator and $\psi_{vk}(\psi_{ck})$ is the wavefunction of valence (conduction) bands. We note that the indirect band transition and intraband absorption is ignored here, not only because their contribution is several orders of magnitude smaller than direct interband transitions, they do not lead to effective valley polarization either due to long absorption timescales and random phonon scattering effects. As shown in figure 2(b), it is observed that the valley optical selection rule to circularly polarized light indeed emerges with $\eta(k) = -1(+1)$ at the $K_+(K_-)$ valley, therefore allowing the circularly polarized light to selectively inject photocarriers into one of the two valleys.

In addition to complicated conventional approach using circularly-polarized light, a unique advantage of magnetic VSe_2 is that valley polarization can also be achieved by easier methods such as hole doping and illumination with light of proper energy, thanks to the emergence of intrinsic valley energy splitting. Figure 3 shows the dependence of band occupation on the doping concentration of 0, 6.2×1013 $|e|\cdot \mathrm{cm}^{-2}$, 10.4×1013 $|e|\cdot \mathrm{cm}^{-2}$, respectively. For hole concentration lower than 6.2×1013 $|e|\cdot \mathrm{cm}^{-2}$, the K_+ valley is unoccupied while the K_- valley is fully occupied. Thus the net valley polarization is achieved. When the hole concentration further increases to $10.4 \times 1013|e|\cdot \mathrm{cm}^{-2}$, both valleys and the hole pocket at Γ will become partially occupied. Therefore, hole doping can bring a nonequilibrium electron occupation between K_- and K_+ valleys, which generate a net transverse current in 2H monolayer VSe_2 by in-plane electric field. It is worth mentioning that the valley splitting remains nearly unchanged for all doping concentration (the variation is less 0.3 meV), indicating the valley property is robust against hole doping. Besides, we expect that hole doping can be easily achieved via organic molecule adsorption on VSe_2 monolayers. About $0.2e$–$0.3e$ per molecule transferred from graphene to electron-accepting molecules TCNQ and F4-TCNQ has been successfully achieved [45]. In addition, intrinsic charge carriers introduced by thermal excitation is sufficient to achieve valley polarization at room temperature.

The valley polarization can also be achieved by proper light illumination without considering optical selection rules. The energy difference $\Delta E_v^c(k) = E_c(k) - E_v(k)$, which is defined as the direct subtraction between conduction band energy and valence band energy, is obtained by using the Wannier interpolation, as shown in figure 4(a). Only focusing on the direct transition from valence band to conduction band, the energy difference equals the photon energy that is used to excite VSe_2. The energy minimum at K_+ (K_-) valley

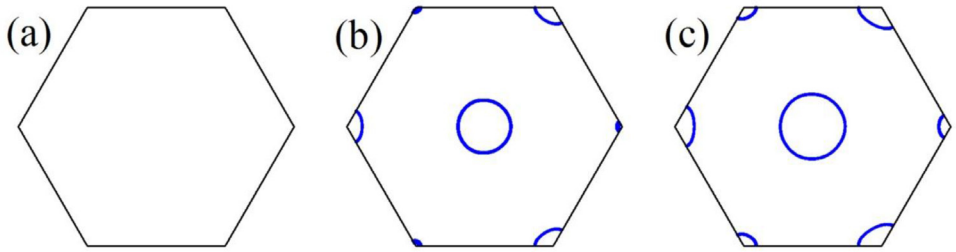

Figure 3. The Fermi surface at the hole doping concentration of 0, $6.2 \times 10^{13}|e|\cdot\mathrm{cm}^{-2}$, $10.4 \times 10^{13}\,|e|\cdot\mathrm{cm}^{-2}$, respectively.

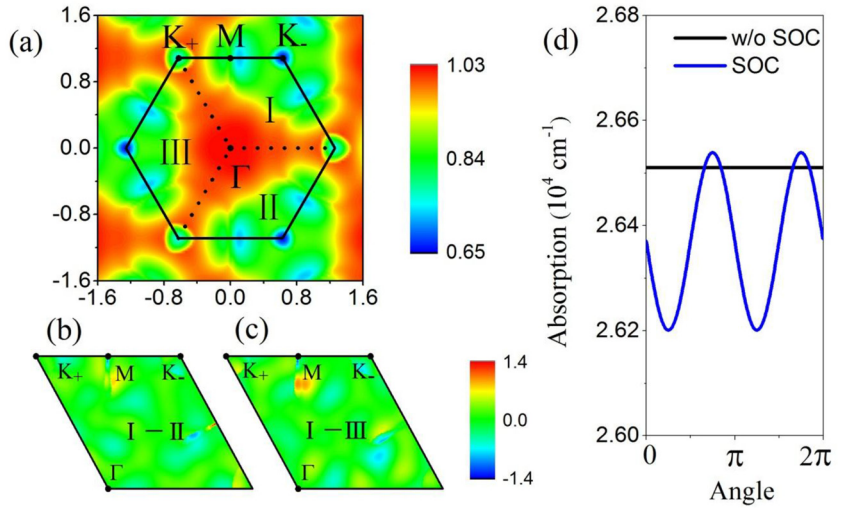

Figure 4. (a) The energy difference (in unit of eV) between the top of the valence band and the bottom of the conduction band. (b) and (c) The energy difference (in unit of meV) between the (II, III) and I part, respectively. (d) The angle-dependent absorption coefficient at a certain energy without SOC (black) and with SOC (blue) effect, respectively.

is 0.75 eV (0.66 eV) with PBE method, and can increase to 0.91 eV (0.78 eV) with hybrid HSE06 functional. Therefore if light with a proper photon energy of 0.78 eV (wavelength 1590 nm) is used to photoexcite VSe_2, only the K_- valley will be excited, generating a valley-polarized carriers. Therefore, light with appropriate photon energy can also be used to produce valley polarization.

The presence of SOC induces not only intrinsic valley splitting due to the broken IS and TRS, more interestingly, it also breaks the three-fold rotational symmetry in electronic structures. Based on the three-fold rotational symmetry of the crystal structure in 2H monolayer VSe_2, ΔE_v^c at the first BZ in figure 4(a) can be divided into three parts, named $\Delta E_v^c(\mathrm{I})$, $\Delta E_v^c(\mathrm{II})$, $\Delta E_v^c(\mathrm{III})$, respectively. The difference $\Delta E_v^c(\mathrm{I}-\mathrm{II})$ and $\Delta E_v^c(\mathrm{I}-\mathrm{III})$, as illustrated in figures 4(b) and (c), shows that ΔE_v^c at the three parts are not completely coincident, which is against the demand of three-fold rotational symmetry in atomic structure. The difference is more prominent around the *M* points. The breaking of three-fold symmetry is a result of SOC in the electronic interactions in the magnetic VSe_2.

The breaking of three-fold rotational symmetry also exhibits itself in the optical absorption properties of VSe_2. We find that the off-diagonal term of dielectric function is nonzero when SOC effect is included in calculation. To see straightforwardly the effect of the off-diagonal term of the absorption coefficient, we calculate angle-dependent absorption spectrum. The absorption coefficient with and without SOC effect calculated by HSE06 functional is shown in figure S3. Assuming the following two equivalent cases: (a) 2H monolayer VSe_2 sample is rotated from 0 to 2π radian, but the linearly polarized light keeps still; (b) the linearly polarized light is rotated while the sample stays the same. For simplicity, only the angle-dependent absorption coefficient at *xx* direction $\alpha_{xx}(\theta)$ is considered (other terms are similar), which can be rewritten as,

$$\alpha_{xx}(\theta) = \cos^2(\theta)\cdot\alpha_{xx} + \sin^2(\theta)\cdot\alpha_{yy} - 2\sin(\theta)\cos(\theta)\cdot\alpha_{xy}, \tag{3}$$

where α_{xx}, α_{yy} and α_{xy} are the absorption coefficient component at three direction for $\theta = 0$, respectively. Here *x* direction denotes the direction of V–V bond in the VSe_2 layer, and the rotation angle θ is the angle between the *x* direction and the polarization direction of linearly polarized lights. The $\alpha_{xx}(\theta)$ is the absorption coefficient at *x* direction at a given rotation angle. The first absorption peak is located at the corresponding energy of 1.41 eV (SI, figure S3), which is chosen to obtain $\alpha_{xx}(\theta)$.

As figure 4(d) illustrates, the light absorption coefficient is isotropic without SOC effect, which meets the demand of the three-fold rotational symmetry of atomic structure ($\alpha_{xx} = \alpha_{yy}, \alpha_{xy} = 0$). However, when the SOC effect is considered, the absorption coefficient shows angle dependence as a result of anomalous appearance of α_{xy}, which means the

breaking of optical isotropy. Due to the equivalent effect of the linearly polarized light along the $+x$ and $-x$ direction, the angle-dependent absorption coefficient shows an oscillating period of π. Combining the analysis of band structure and the angle-dependent absorption coefficient, we conclude that a pure SOC effect can break optical isotropy held by macroscopic crystal symmetry.

The refractive index of a material is directly proportional to the arithmetic square root of complex dielectric constant. Our results show that the complex dielectric constant along the *xx* and *yy* directions is the same without SOC effect, meaning the equivalent refractive index of the two directions, so no light deflection happens. However, the complex dielectric constant is anisotropic when SOC is considered, generating an unequal refractive index, then light deflection can be obtained. The intrinsic magnetic moment has almost remained unchanged before and after SOC effect is considered, which can also be treated as an external magnetic field. The above anisotropic phenomenon including the complex dielectric constant and absorption coefficient is induced by SOC, which is different from conventional magneto-optic effect. We estimate from the valley splitting of the valence band with and without SOC that the effective magnetic field associated with SOC amounts to ~700 T for the magnetic VSe_2. This would introduce giant magneto-optic effect that is radically different from conventional ones coming from light–matter interaction.

4. Conclusions

In summary, we have studied the breaking of the valley degeneracy and optical isotropy induced by the SOC effect in 2H magnetic VSe_2 monolayer film by using first-principles calculations. Because of the broken IS and TRS, the valley splitting about 78.2 meV is large enough to obtain the intrinsic valley polarization in monolayer transition metal dichalcogenide at room temperature. Additionally, the valley splitting can be tuned via biaxial strain, providing an effective strategy to realize valley polarization and to manipulate the valley degree of freedom at will.

Acknowledgments

We acknowledge financial support from the National Basic Research Program of China (Grant No. 2016YFA0300902, 2013CBA01600, and 2015CB921001), National Natural Foundation of China (Grant No. 61306114) and 'Strategic Priority Research Program (B)' of Chinese Academy of Sciences (Grant No. XDB07030100).

References

[1] Chang M C and Niu Q 1995 Berry phase, hyperorbits, and the Hofstadter spectrum: semiclassical dynamics in magnetic Bloch bands *Phys. Rev.* B **53** 7010
[2] Sundaram G and Niu Q 1998 Wave-packet dynamics in slowly perturbed crystals: gradient corrections and Berry-phase effects *Phys. Rev.* B **59** 14915
[3] Yao Y, Kleinman L, MacDonald A H, Sinova J, Jungwirth T, Wang D S, Wang E and Niu Q 2004 First principles calculation of anomalous Hall conductivity in ferromagnetic bcc Fe *Phys. Rev. Lett.* **92** 037204
[4] Xiao D, Yao W and Niu Q 2007 Valley-contrasting physics in graphene: magnetic moment and topological transport *Phys. Rev. Lett.* **99** 236809
[5] Yao W, Xiao D and Niu Q 2008 Valley-dependent optoelectronics from inversion symmetry breaking *Phys. Rev.* B **77** 235406
[6] Sun J T, Wang Z, Meng S, Du S, Liu F and Gao H J 2016 Spin-polarized valley Hall effect in ultrathin silicon nanomembrane via interlayer antiferromagnetic coupling *2D Mater.* **3** 035026
[7] Cao T *et al* 2012 Valley-selective circular dichroism of monolayer molybdenum disulphide *Nat. Commun.* **3** 887
[8] Xiao D, Liu G B, Feng W, Xu X and Yao W 2012 Coupled spin and valley physics in monolayers of MoS_2 and other group-VI dichalcogenides *Phys. Rev. Lett.* **108** 196802
[9] Liu G B, Xiao D, Yao Y, Xu X and Yao W 2015 Electronic structures and theoretical modelling of two-dimensional group-VIB transition metal dichalcogenides *Chem. Soc. Rev.* **44** 2643–63
[10] Aivazian G, Gong Z, Jones A M, Chu R L, Yan J, Mandrus D G, Zhang C, Cobden D, Yao W and Xu X 2015 Magnetic control of valley pseudospin in monolayer WSe_2 *Nat. Phys.* **11** 148–52
[11] Li Y *et al* 2014 Valley splitting and polarization by the Zeeman effect in monolayer $MoSe_2$ *Phys. Rev. Lett.* **113** 266804
[12] MacNeill D, Heikes C, Mak K F, Anderson Z, Kormanyos A, Zolyomi V, Park J and Ralph D C 2015 Breaking of valley degeneracy by magnetic field in monolayer $MoSe_2$ *Phys. Rev. Lett.* **114** 037401
[13] Srivastav A, Sidler M, Allain A V, Lembke D S, Kis A and Imamoğlu A 2015 Valley zeeman effect in elementary optical excitations of monolayer WSe_2 *Nat. Phys.* **11** 141–7
[14] Ye Y, Xiao J, Wang H, Ye Z, Zhu H, Zhao M, Wang Y, Zhao J, Yin X and Zhang X 2016 Electrical generation and control of the valley carriers in a monolayer transition metal dichalcogenide *Nat. Nanotechnol.* **11** 598–602
[15] Zeng H, Dai J, Yao W, Xiao D and Cui X 2012 Valley polarization in MoS_2 monolayers by optical pumping *Nat. Nanotechnol.* **7** 490–3
[16] Arora A, Schmidt R, Schneider R, Molas M R, Breslavetz I, Potemski M and Bratschitsch R 2016 Valley zeeman splitting and valley polarization of neutral and charged excitons in monolayer $MoTe_2$ at high magnetic fields *Nano Lett.* **16** 3624–9
[17] Freitag N M *et al* 2016 Electrostatically confined monolayer graphene quantum dots with orbital and valley splittings *Nano Lett.* **16** 5798–805
[18] Miwa J A, Warschkow O, Carter D J, Marks N A, Mazzola F, Simmons M Y and Wells J W 2014 Valley splitting in a silicon quantum device platform *Nano Lett.* **14** 1515–9
[19] Plechinger G *et al* 2016 Excitonic valley effects in monolayer WS_2 under high magnetic fields *Nano Lett.* **16** 7899–904
[20] Sanchez O L, Ovchinnikov D, Misra S, Allain A and Kis A 2016 Valley polarization by spin injection in a light-emitting van der Waals heterojunction *Nano Lett.* **16** 5792–7
[21] Song X, Xie S, Kang K, Park J and Sih V 2016 Long-lived hole spin/valley polarization probed by Kerr rotation in monolayer WSe_2 *Nano Lett.* **16** 5010–4
[22] Yang W *et al* 2016 Electrically tunable valley-light emitting diode (vLED) based on CVD-grown monolayer WS_2 *Nano Lett.* **16** 1560–7
[23] Tong W Y, Ding H C, Gao Y C, Gong S J, Wan X and Duan C G 2014 Spin-dependent optical response of

multiferroic EuO: first-principles DFT calculations *Phys. Rev.* B **89** 064404
[24] Qi J S, Li X, Niu Q and Feng J 2015 Giant and tunable valley degeneracy splitting in $MoTe_2$ *Phys. Rev.* B **92** 121403
[25] Ma Y D, Dai Y, Guo M, Niu C W, Zhu Y T and Huang B B 2012 Evidence of the existence of magnetism in pristine VX_2 monolayers (X = S, Se) and their strain-induced tunable magnetic properties *ACS Nano* **6** 1695–701
[26] Wasey A H M A, Chakrabarty S and Das G P 2015 Quantum size effects in layered VX_2 (X = S, Se) materials: manifestation of metal to semimetal or semiconductor transition *J. Appl. Phys.* **117** 064313
[27] Zhang H, Liu L M and Lau W M 2013 Dimension-dependent phase transition and magnetic properties of VS_2 *J. Mater. Chem.* A **1** 10821
[28] Kan M, Wang B, Lee Y H and Sun Q 2014 Tunable structure, magnetism and metal-insulator phase transition in VS_2 monolayer induced by in-plane biaxial strain *Nano Res.* **8** 1348–56
[29] Feng J, Sun X, Wu C, Peng L, Lin C, Hu S, Yang J and Xie Y 2011 Metallic few-layered VS_2 ultrathin nanosheets: high two-dimensional conductivity for in-plane supercapacitors *J. Am. Chem. Soc.* **133** 17832–8
[30] Zhao W, Dong B, Guo Z, Su G, Gao R, Wang W and Cao L 2016 Colloidal synthesis of VSe_2 single-layer nanosheets as novel electrocatalysts for the hydrogen evolution reaction *Chem. Commun.* **52** 9228–31
[31] Tong W Y, Gong S J, Wan X G and Duan C G 2016 Concepts of ferrovalley material and anomalous valley Hall effect *Nat. Commun.* **7** 13612
[32] Kresse G 1996 Efficient iterative schemes for *ab initio* total-energy calculations using a plane-wave basis set *Phys. Rev.* B **54** 11169
[33] Kresse G 1999 From ultrasoft pseudopotentials to the projector augmented-wave method *Phys. Rev.* B **59** 1758
[34] Blöchl P E 1994 Projector augmented-wave method *Phys. Rev.* B **50** 17953–79
[35] Perdew J P, Burke K and Ernzerhof M 1996 Generalized gradient approximation made simple *Phys. Rev. Lett.* **77** 3865
[36] Heyd J, Scuseria G E and Ernzerhof M 2003 Hybrid functionals based on a screened coulomb potential *J. Chem. Phys.* **118** 8207
[37] Monkhorst H J and Pack J D 1976 Special points for Brillouin-zone integrations *Phys. Rev.* B **13** 5188–92
[38] Hobbs D, Kresse G and Hafner J 2000 Fully unconstrained noncollinear magnetism within the projector augmented-wave method *Phys. Rev.* B **62** 11556
[39] Mostofi A A, Yates J R, Lee Y S, Souza I, Vanderbilt D and Marzari N 2008 Wannier90: a tool for obtaining maximally-localised Wannier functions *Comput. Phys. Commun.* **178** 685–99
[40] Kudrnovsky J, Turek I, Drchal V, Maca F, Weinberger P and Bruno P 2004 Exchange interactions in III–V and group-IV diluted magnetic semiconductors *Phys. Rev.* B **69** 115208
[41] Liu G B, Shan W Y, Yao Y, Yao W and Xiao D 2013 Three-band tight-binding model for monolayers of group-VIB transition metal dichalcogenides *Phys. Rev.* B **88** 085433
[42] Cao T, Li Z and Louie S G 2015 Tunable magnetism and half-metallicity in hole-doped monolayer GaSe *Phys. Rev. Lett.* **114** 236602
[43] Bardeen J and Shockley W 1950 Deformation potentials and mobilities in non-polar crystals *Phys. Rev.* **80** 72–80
[44] Feng W, Yao Y, Zhu W, Zhou J, Yao W and Xiao D 2012 Intrinsic spin Hall effect in monolayers of group-VI dichalcogenides: a first-principles study *Phys. Rev.* B **86** 165108
[45] Sun J T, Lu Y H, Chen W, Feng Y P and Wee A T S 2010 Linear tuning of charge carriers in graphene by organic molecules and charge-transfer complexes *Phys. Rev.* B **81** 155403